A stability vulnerability in the interaction between Volt-VAR and Volt-Watt response functions for smart inverters

Julio H. Braslavsky, John K. Ward and Lyle Collins

Abstract— **The strong uptake of PV systems, both within Australia and internationally, and particularly for small-scale systems within residential distribution networks, has raised concerns over potential impacts such as over-voltages. Responding to these potential issues, distribution network operators are beginning to impose restrictions on PV installations, including limiting system size, ramp rates, and exporting and managing reactive power. Additionally, inverter standards (such as AS/NZS 4777) are being updated with revised power quality functionality such as Volt-VAR and Volt-Watt control functions. This paper considers a specific case of the interaction between Volt-VAR and Volt-Watt inverter functions and demonstrates, both analytically and via a simulation example, that this interaction can lead to voltage instability if not adequately designed.**

I. INTRODUCTION

The energy sector is in the midst of a fundamental transformation. Internationally, Germany now has PV penetration of around 50% of peak electricity capacity [1], while in Australia PV is installed on over one million homes, contributing over 10% of the peak National Energy Market (NEM) capacity. Energy usage patterns are also changing and in Australia the increasing uptake of air-conditioning systems has substantially driven peak demand growth, due to the high correlation between air-conditioning loads.

Within Australia, the combined impact of (predominately) PV and air-conditioning uptake within residential distribution networks has increased the range of daily power flows leading to larger voltage swings and issues of over-voltages [2, p. 75]. Further compounding this has been a trend of reduced energy consumption, which has grown peak demand relative to energy consumption and undermined energy based revenue structures for network operators.

One response to these conditions has been that network operators in some areas have begun restricting the size of PV system installations and requiring ramp rate limits, inclusion of energy storage, and reactive power control [3], [4].

Another response has been the development of smart inverter power quality functions, where inverters can automatically change their real and reactive power setpoints to help manage network power quality. Two key functions here are Volt-Watt and Volt-VAR responses, such as described in the Electric Power Research Institute (EPRI) report on smart inverter functions [5], and now being implemented into inverter standards — such as the upcoming revisions to AS/NZS4777.

The authors are with the Energy Flagship, Australian Commonwealth Scientific and Industrial Research Organisation (CSIRO). Braslavsky and Collins are also with the School of EE&CS, The University of Newcastle.

Peak PV generation around noon is significantly higher than typical customer loads, which may lead to over-voltages. Figure 1 shows an example average load and (normalised) PV generation profile from over 7000 customers as collected as part of the Ausgrid Smart Grid Smart City (SGSC) project [6]. Since the average peak capacity of PV installations in Australia is around 2.5kW[7], it is apparent from this figure that voltage rise issues are likely already in some areas.

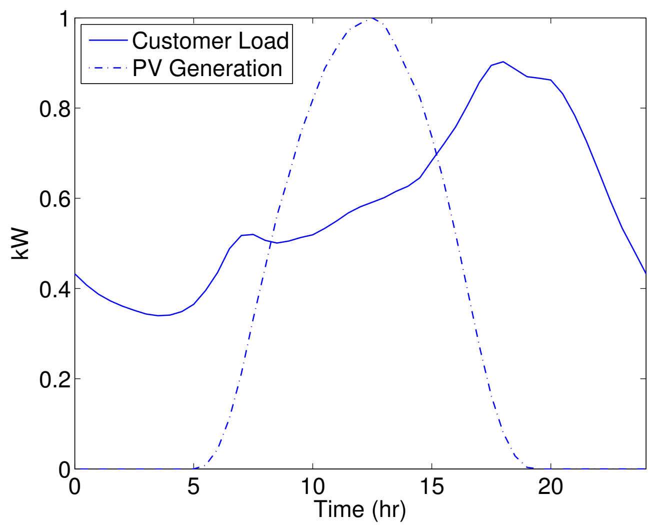

Fig. 1. Average residential load versus normalised PV generation

In addition to the potential for voltage rise during periods of high solar insolation, other contributing factors include the facts that: (1) PV panels are rated based on a nominal $1000\mathrm{W/m^2}$irradiance level, and that this level if often exceeding in Australia; and (2) system design practices often size the inverter to be significantly smaller than the DC PV panel rating, to account for factors such as imbalances, inefficiencies, losses. As an example of (1), Figure 2 shows the proportion of time where solar irradiance exceeds a given level at various locations around Australia, based on several years worth of 1-minute data [8]. As an example of (2), the Clean Energy Council design guide for grid connected PV systems recommends that inverters be sized at greater than 75% of the PV array peak power.

The significance of these factors is that there is likely a significant portion of time during times of high solar insolation when PV inverters are operating at their rated capacity and network voltage are high, triggering both Volt-VAR and Volt-Watt power quality functions. This paper considers this specific case of the interaction between Volt-VAR and Volt-

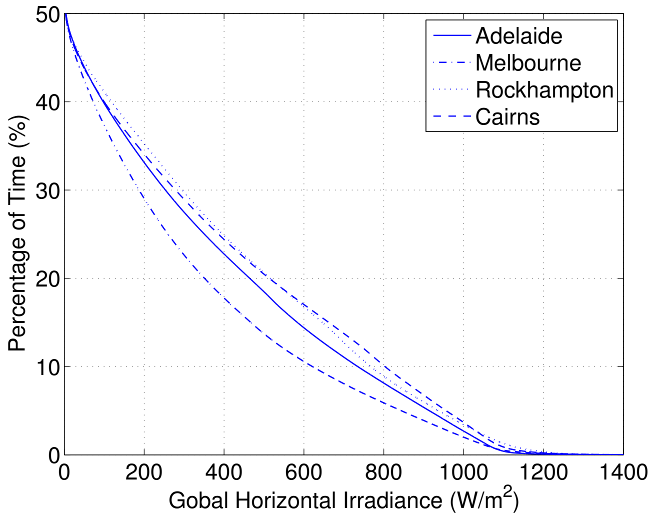

Fig. 2. Proportion of time PV irradiance exceeds given levels.

Watt inverter functions while the inverter is operating at maximum capacity, and demonstrates, both analytically and via a simulation example, that under this specific scenario, *this interaction can lead to a voltage instability*.

A key implication of the analysis in this paper is the importance of the *precedence* between Volt-Watt and Volt-VAR functions of the inverter at times when both functions are active. According to the EPRI report [5], Watt output takes precedence over VARs in the context of the "Intelligent Volt-VAR Function", namely, the "Available VARs" in the Volt-VAR curves are, irrespective of the capability of the energy resource at the moment, without compromising Watt output. This is the case in the two scenarios considered in [5] to illustrate the interaction between the Volt-Watt Function with the intelligent Volt-VAR function. The report proposes that "Watts takes precedence over VAR" in that any VAR level requested is coupled to the the Volt-Watt function so that if the inverter is producing at full Watt capacity, no VARs are generated. The Volt-VAR function then generates VARs as percent of available VAR capability.

The problem with this proposed precedence of Watts over VARs is that when the inverter is generating Watts to 100% of its limit, the effective slope at which VARs will start to be injected when the Volt-Watt function is activated may effectively be infinite, which introduces a voltage stability vulnerability, as we will show in the present paper.

There has been relatively little analysis done on stability issues arising from the implementation of Volt-VAR functions, and apparently no stability analysis exists on the joint implementation of Volt-VAR and Volt-Watt inverter functions, which is the focus of the present paper. Stability issues associated the implementation of a Volt-VAR function to mitigate over-voltage have been recently discussed in [9]. However the analysis in [9] points to instability introduced by delay measurements in the control loop. In another recent study, [10] considered instabilities due to Volt-VAR functions with time-delays through numerical simulations. No real power curtailment is considered in these references.

This paper rigorously exposes a stability vulnerability that is intrinsic to the interaction between Volt-VAR and Volt-Watt functions. We develop the analytical framework to study the nonlinear dynamics arising in a single inverter with Volt-VARs and Volt-Watts functions connected through a lossy line to the grid, which is modelled as an infinite bus that regulates frequency and voltage. The main results are analytic conditions for the existence of an equilibrium voltage within a critical region, and a characterisation of its stability in terms of the parameters of the inverter, the line, and the grid. Proofs are omitted due to space limitations and will be included in a journal submission currently under preparation. The results are illustrated on a numerical simulation example derived from [9].

Section II defines the system under study and develops an analytic framework to formulate the main results, given in Section II-C. Section III presents a simulation example, and Section IV presents conclusions and discusses future work.

II. STABILITY ANALYSIS

A. System model

Consider a single-phase inverter connected to a power grid through an inductive line impedance $Z\angle\theta = R+jX$, $X > 0$, as shown in the schematics of Figure 3.

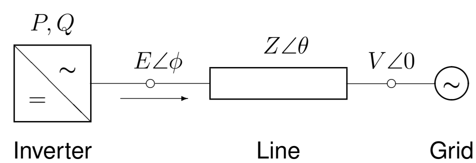

Fig. 3. Single-phase inverter connected to an infinite bus grid.

The inverter injects active and reactive powers P and Q at its point of connection to the grid at a voltage $E\angle\phi$. The grid, modelled as an infinite bus, is assumed to regulate the supplied frequency and voltage $V\angle 0$, which is taken as phase reference. The inverter has Volt-VAR and Volt-Watt voltage support capabilities, which will inject or absorb reactive power, and curtail active power injection when the voltage amplitude E exceeds admissible levels.

The (complex) current injected by the inverter is given by

$$I = (G + jB)(Ee^{j\phi} - V), \tag{1}$$

where $G + jB = Y = Z^{-1}$ is the line admittance, with $G = R/(R^2 + X^2)$ and $B = -X/(R^2 + X^2)$. The complex power $S = P + jQ$ injected by the inverter is given by

$$S = I^* Ee^{j\phi}, \tag{2}$$

which, by substitution of I from (1), yields

$$\begin{aligned} S &= (G - jB)(Ee^{-j\phi} - V)Ee^{j\phi} \\ &= (G - jB)(E^2 - VEe^{j\phi}). \end{aligned} \tag{3}$$

Using the fact that $e^{j\phi} = \cos\phi + j\sin\phi$, Equation (3) can be separated into its real and imaginary parts, which leads to the power flow equations

$$P = E^2G - VE(G\cos\phi + B\sin\phi), \quad (4)$$
$$Q = -E^2B - VE(G\sin\phi - B\cos\phi). \quad (5)$$

Equations (4) and (5) can be manipulated to eliminate the dependency on ϕ and express a relationship between the inverter voltage E, the grid voltage V, the injected powers P and Q, and the line parameters, which yields the equation

$$E^4 - [2(PR+QX)+V^2]E^2 + (P^2+Q^2)(R^2+X^2) = 0. \quad (6)$$

The voltage drop between two nodes, $E^2 - V^2 = 2(PR+QX) - (R^2+X^2)(P^2+Q^2)/E^2$, as obtained in conventional branch flow equations [11], [12], follows directly from (6).

B. Volt-VAR and Volt-Watt inverter functions

We consider an inverter with voltage Volt-Watt and Volt-VAR support functions. These functions trigger the injection of reactive power and the curtailment of active power when the voltage is beyond the normal operation range. These functions dynamically compute reference values for the injected powers P and Q as functions of the voltage magnitude E at the inverter point of connection to the grid, and are typically considered as sectionally linear droop characteristics as shown in Figures 5 and 4 [5, §9 and §10].

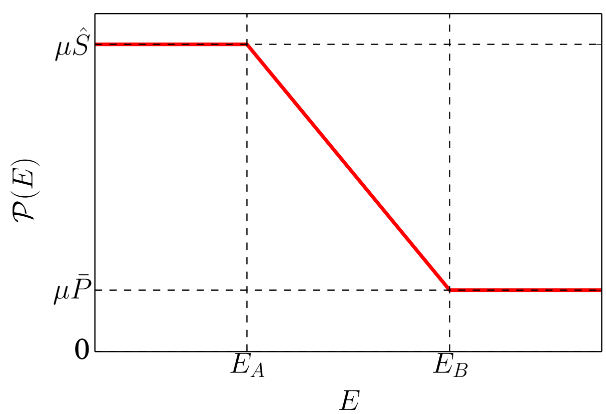

Fig. 4. The Volt-Watt function.

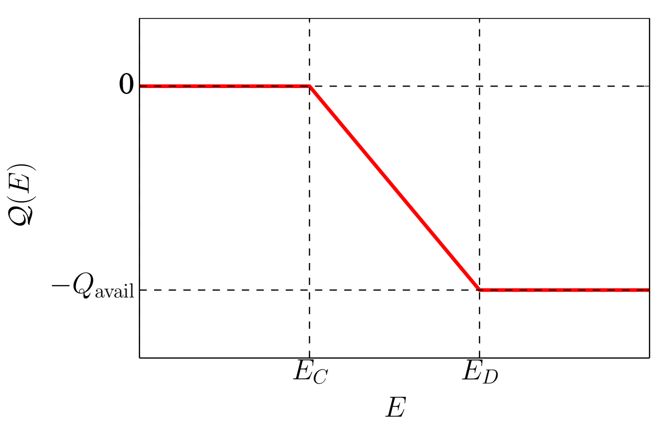

Fig. 5. The Volt-VAR function.

The Volt-Watt function $\mathcal{P}(E)$ in Figure 4 is defined as

$$\mathcal{P}(E) = \begin{cases} \mu\hat{S} & \text{if } E \le E_A, \\ \mu\hat{S}\big(1 - d(E - E_A)\big) & \text{if } E \in [E_A, E_B], \\ \mu\hat{S}\big(1 - d(E_B - E_A)\big) & \text{if } E_B \le E. \end{cases} \quad (7)$$

where $\bar{\mu} \le \mu \le 1$ is a parameter that represents the fractional amount of the active power that can be injected by the inverter relative to its rated apparent power, assumed greater than a minimum value $\bar{\mu}$, to be more precisely specified below. In referring to Figure 4, $\bar{P} = \hat{S}(1 - d(E_B - E_A))$. The droop coefficient d and trigger voltages E_A and E_B are also design parameters of the function.

The Volt-Watt function defined in (7) operates on a *dynamic* maximum reference setpoint, where the active power curtailment occurs relative to the inverter operating point at the time that the over-voltage condition occurs [13] (see also [14], [15]). It is important to note that the stability vulnerability presented in this paper can happen if the Volt-Watt function is defined with the (simpler) *static* maximum reference setpoint. For the static maximum type inverter model, the E_A and E_B parameters can be considered functions of the available real power.

The Volt-VAR function $\mathcal{Q}(E)$ in Figure 5 is defined as

$$\mathcal{Q}(E) = \begin{cases} 0 & \text{if } E \le E_C, \\ -Q_{\text{avail}}\frac{(E-E_C)}{(E_D-E_C)} & \text{if } E \in [E_C, E_D], \\ -Q_{\text{avail}} & \text{if } E_D \le E, \end{cases} \quad (8)$$

where the trigger voltages E_C and E_D are design parameters. In this paper we focus on the case of over-voltage, where typically negative VARs would need to be injected. The maximum level of reactive power injection $\hat{Q}$ is often limited so that (for the operating region specified) the inverter power factor $\cos\delta = P/\hat{S}$ does not fall below admissible limits, for example $\cos\delta \ge \cos\bar{\delta} = 0.90$. The injected reactive power is also limited to the *available* capacity Q_{avail} given the inverter apparent power capacity and the current level of active power injection [9], [12], [13], [16], namely,

$$Q_{\text{avail}} = \min\left\{\hat{Q}, \sqrt{\hat{S}^2 - \mathcal{P}(E)^2}\right\}. \quad (9)$$

The mode in which the maximum allowed real power output is attained (regardless of whether the reactive power operating point can be achieved) is referred to as the *real power preferred* response in [13].

We assume that the system operates at a voltage $E \ge E_A$, where $E_A \ge E_D$. The analysis in the sequel is limited to the (most critical) range of voltages E at which the inverter sustains full injection of its rated apparent power $\hat{S}$ as either real power, reactive power, or a combination of both. Namely,

$$\mathcal{P}(E)^2 + \mathcal{Q}(E)^2 = \hat{S}^2 \quad \text{for all } E \le \hat{E}, \quad (10)$$

where $\hat{E}$ is such that in (9)

$$Q_{\text{avail}} = \sqrt{\hat{S}^2 - \mathcal{P}(E)^2} \le \hat{Q}, \quad \forall E \le \hat{E}.$$

The value of $\hat{E}$ may be obtained from (7) since

$$\mu\hat{S}\big(1-d(E-E_A)\big)=\mathcal{P}(E)\geq\sqrt{\hat{S}^2-\hat{Q}^2},$$

which means that

$$E\leq E_A+\frac{1}{d}\left(1-\frac{\bar{\mu}}{\mu}\right)\doteq\hat{E}, \tag{11}$$

where

$$\bar{\mu}\doteq\sqrt{1-\frac{\hat{Q}^2}{\hat{S}^2}}=\cos\bar{\delta} \tag{12}$$

is the minimum value of μ for which (10) is satisfied at $E=E_A$ (note that $\hat{E}=E_A$ when $\mu=\bar{\mu}$).

We further assume that $\hat{E}\leq E_B$ in (7), and that $\mu\in[\bar{\mu},1]$, so that for the case considered, (7), (8), (9) reduce to

$$\begin{aligned}\mathcal{P}(E)&=\mu\hat{S}(1-d(E-E_A)),\\ \mathcal{Q}(E)&=-\sqrt{\hat{S}^2-\mathcal{P}(E)^2},\\ E&\in[E_A,\hat{E}],\quad \mu\in[\bar{\mu},1].\end{aligned} \tag{13}$$

C. Stability issues in Volt-VAR and Volt-Watt responses

To analyse the dynamic interaction between the Volt-VAR and Volt-Watt inverter functions, the measurement of the voltage E_k, required to compute the injected powers through (7) and (8), is modelled as the discrete-time low-pass filter

$$E_{k+1}=aE_k+(1-a)F(E_k), \tag{14}$$

where a is a real constant with magnitude $|a|<1$, which guarantees bounded-input bounded-output stability of the measurement, and the function $F(E_k)$ is defined as

$$F(E_k)=\sqrt{G(E_k)+{}^{V^2}\!/_2+\sqrt{\left(G(E_k)+{}^{V^2}\!/_2\right)^2-\hat{S}^2Z^2}} \tag{15}$$

where $G(E_k)=R\mathcal{P}(E_k)+X\mathcal{Q}(E_k)$.

The low-pass filter dynamics (14) represent typical behaviour of real-world inverters, intended to limit the rate of change of the Volt-Watt and Volt-VAR inverter functions [5].

The nonlinear function $F(E_k)$ arises in the form of the solution $x=b/2+\sqrt{b^2/4-c}$ to (6) viewed as $x^4-bx^2+c=0$, and is used to guarantee that the algebraic relation (6) is satisfied at any equilibrium of (14). This follows from the fact that any fixed point $E^*=F(E^*)$ represents a solution of (6) after substituting $P=\mathcal{P}(E), Q=\mathcal{Q}(E)$, and $P^2+Q^2=\hat{S}^2$, which holds for $E\in[E_A,\hat{E}]$. Such fixed point is an equilibrium of the nonlinear closed-loop dynamic system obtained by substituting (13) in (15) and then (14), since if $E_k=E^*=F(E^*)$, then $E_{k+1}=aE^*+(1-a)E^*=E^*$.

The existence of such equilibrium within the range $E\in[E_A,\hat{E}]$ can be shown from continuity and monotonicity of the function $F(E)$ in this range.

Lemma 1 (Existence of an equilibrium voltage): Consider an inverter with maximum rated apparent power $\hat{S}$ and maximum reactive power $\hat{Q}$, which is connected by a line with impedance $Z\angle\theta=R+jX$ to a grid with voltage V. Let $\hat{E}$ and $\bar{\mu}$ be as per (11) and (12) and suppose that

$$F(E_A)\geq E_A\quad\text{and}\quad F(\hat{E})\leq\hat{E}. \tag{16}$$

Then the dynamic system formed by (14) under the conditions (13) has a unique equilibrium $E^*\in[E_A,\hat{E}]$.

Figure 6 illustrates typical shapes of $F(E),\mathcal{Q}(E)$ and $\mathcal{P}(E)$ for $\mu=1$. Notice the sharp decrease in $\mathcal{Q}(E)$ at the point $E=E_A$, when the droop in $\mathcal{P}(E)$ becomes active.

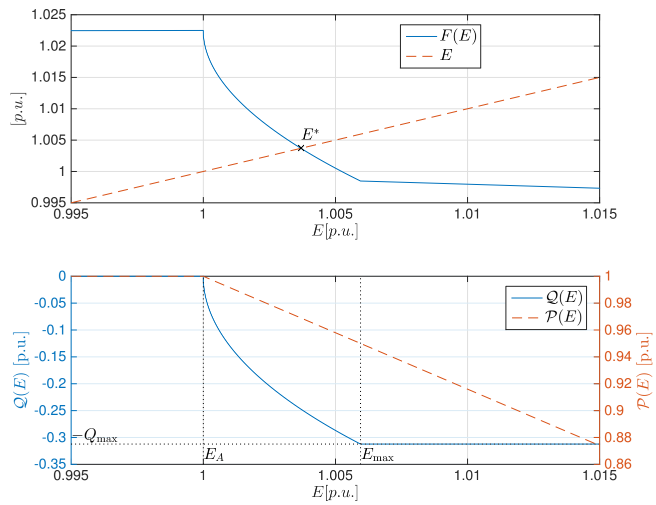

Fig. 6. Plot of $F(E)$ (top), $\mathcal{Q}(E)$ and $\mathcal{P}(E)$ (bottom) for $\mu=1$.

The local stability of the equilibrium E^* of (14) may be determined by analysing the magnitude of its Jacobian evaluated at E^*, namely

$$\rho=\left|a+(1-a)\frac{\partial F(E)}{\partial E}\bigg|_{E^*}\right|. \tag{17}$$

We can see from the top plot in Figure 6 that if the equilibrium E^* occurs sufficiently close to E_A, then the slope $\partial F(E)/\partial E|_{E^*}$ might have a magnitude sufficiently high to cause instability, which is more likely when μ is closer to 1. The following fact gives an analytic expression of the Jacobian of $F(E)$ derived from (15) under (13).

Fact 1 (Jacobian of $F(E_k)$): For any voltage E_k in the interval $[E_A,\hat{E}]$, the Jacobian of $F(E_k)$ in (15) is given by

$$\frac{\partial F(E_k)}{\partial E_k}=\frac{G'(E_k)F(E_k)}{2\sqrt{\left(G(E_k)+{}^{V^2}\!/_2\right)^2-\hat{S}^2Z^2}}. \tag{18}$$

The stability of the equilibrium E^* of (14) under (13) is then characterised using Lyapunov's indirect method.

Theorem 1 (Voltage stability): Consider the conditions of Lemma 1 and let ρ be given by (17). Then,

(a) If $\rho<1$ the equilibrium E^* is exponentially stable.

(b) If $\rho>1$ the equilibrium E^* is unstable.

Sufficient conditions for the stability and instability of the equilibrium E^* can be obtained by analytically bounding the Jacobian expression (18) when $F(E_k)$ is convex on $[E_A,\hat{E}]$.

Corollary 1: Assuming $F(E_k)$ is convex on $[E_A,\hat{E}]$, and under the conditions of Theorem 1,

(a) The equilibrium E^* of (14) is exponentially stable if

$$\mu \hat{S} d\left(X\frac{\mu}{\sqrt{1-\mu^2}}+R\right)F(E_A) < 2\sqrt{\left(G(E_A)+{}^{V^2}\!/_2\right)^2-\hat{S}^2Z^2}\left(\frac{1+a}{1-a}\right). \quad (19)$$

(b) The equilibrium E^* of (14) is unstable if

$$\mu \hat{S} d\left(X\frac{\bar{\mu}}{\sqrt{1-\bar{\mu}^2}}+R\right)F(\hat{E}) > 2\sqrt{\left(G(\hat{E})+{}^{V^2}\!/_2\right)^2-\hat{S}^2Z^2}\left(\frac{1+a}{1-a}\right). \quad (20)$$

III. PRACTICAL EXAMPLE

This example is largely derived from [9], which uses the American electricity grid as design reference. As the ratio

$$\frac{\sqrt{\left(G(E_k)+{}^{V^2}\!/_2\right)^2-\hat{S}^2Z^2}}{F(E_k)} \quad (21)$$

strictly increases as a function of the external grid voltage (V), instability is more likely occur if the nominal voltage is relatively low (inequality 20). In accordance with Figure 7, a two-bus system was simulated using the open source electrical power flow program PYPOWER [18]. The parameters are shown below in Table I.

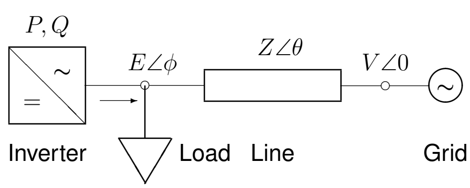

Fig. 7. A single phase inverter and load connected to the external grid through a line impedance.

TABLE I
PARAMETERS FOR THE BASE-CASE SCENARIO.

Parameter	Value	Parameter	Value
V	129 V	d	12.0
E_A	125 V	E_B	135 V
R	0.076 Ω	X	0.268 Ω
$\hat{S}$	1500 VA	a	0.25
μ	0.990	$\cos\bar{\delta}$	0.90
P_L	3000 W	Q_L	1000 VAR

The base case scenario is very close to being marginally stable as shown in Figure 8, with comparison against other values of μ. As shown, the system is very sensitive to small changes in μ, indicating that instability becomes more likely when the inverter operates closer to capacity. An arbitrary limit on the maximum reactive power to be exported by the inverter has been enforced (i.e. $\cos\bar{\delta} = 0.90$) to maintain an inverter power factor appropriately close to 1. The excursions of the voltage into the adjacent control region is not of importance, as the Volt-Watt function in this region has been included in the simulation (thus the accuracy of the simulation is maintained). Note that it is assumed that $E_D \ll E_A$ such that the slope of the Volt-VAR function between E_C and E_D is ignored.

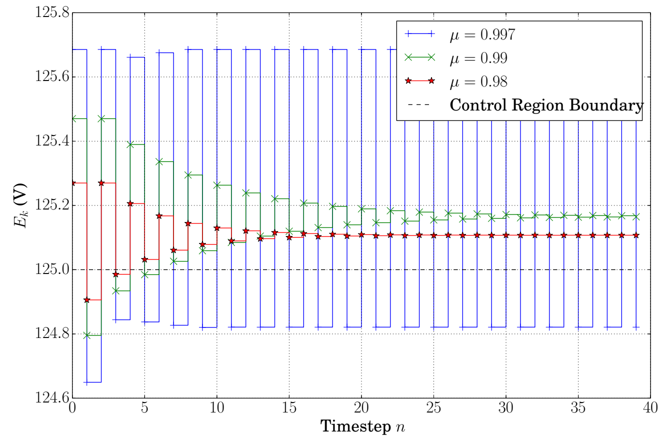

Fig. 8. Voltage stability as a function of μ.

The resistance of low voltage lines can be significantly greater than that of high voltage lines, such that the approximation of a distribution line as having negligible resistance may not be realistic [19]. For the circumstances of this example, increasing the resistance of a distribution line has a damping effect, which reduces the magnitude of the oscillations in voltage (as shown in Figure 9) and power (both real and reactive). Noting that the apparent power consumed by the load is greater than that produced by the inverter, the increase in the resistance has the effect of increasing the voltage drop between the inverter and the grid. The drop increases until such a point in which the voltage equilibrium E^* is moved into the adjacent control region, in which case asymptotic stability is maintained.

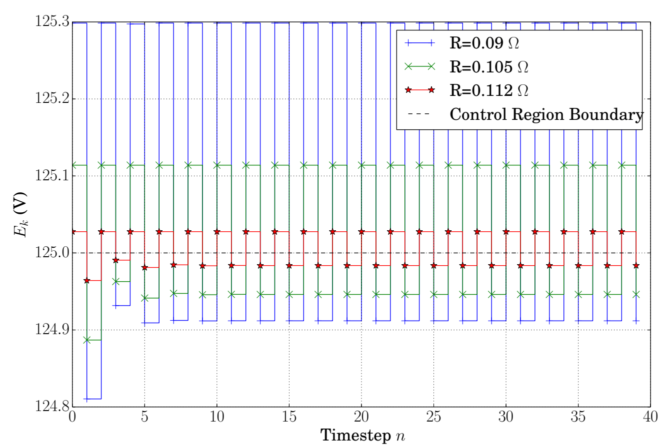

Fig. 9. Voltage stability as a function of R.

The bandwidth of the voltage measurement filter, characterised by a, is important to maintaining stability. As expected from Corollary 1(b) and demonstrated in Figure 10, if the filter is too fast instability results. The filter parameter, a needs to be selected such that $|a| < 1$ for open loop BIBO stability, with a lower value indicating a faster system.

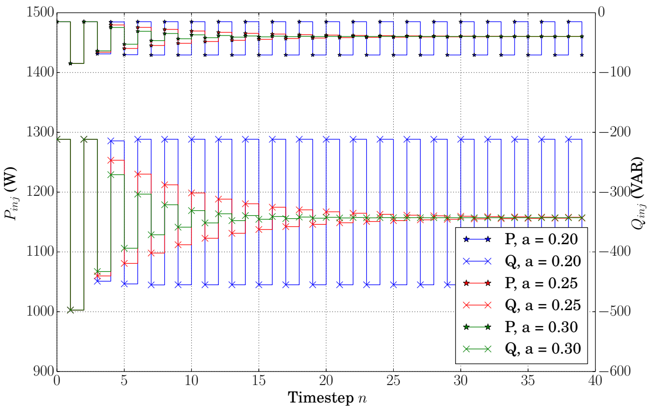

Fig. 10. Real and reactive power dynamics as a function of the voltage filter coefficient.

IV. CONCLUSIONS

Increasing levels of PV system deployments within electricity distribution networks has led to concern of over-voltage conditions, which are especially likely at times of high solar insolation when inverters are running at near full rated capacity. To help address this issue, reactive power control can be used to regulate voltage, and this is typically implemented by means of a Volt-VAR function. Whilst convenient and simple, when used in conjunction with a Volt-Watt function, we have shown that this presents a potential stability issue. Not only does this potential for instability exist, but given that design guidelines recommend undersizing of inverters relative to PV panel ratings [20], this instability is likely to occur. *To the best of the authors' knowledge, this vulnerability was previously unknown*.

This paper has presented a rigorous analysis that establishes (tight) conditions to determine exponential stability and instability. This instability is a function of the design parameters chosen, specifically the measurement filter parameters as well as the Volt-Watt and Volt-VAR functions, and the specific operating conditions considered.

Though not the focus of this paper, potential solutions could include the introduction of smoother Volt-Watt and Volt-VAR functions, as well as over-sizing inverters. This, and other solutions are the subject of ongoing research.

V. ACKNOWLEDGMENTS

This project received funding from ARENA, the Australian Renewable Energy Agency, which the authors gratefully acknowledge. The views expressed herein are the authors' and not necessarily the views of the Australian Government, and the Australian Government does not accept responsibility for any information or advice contained herein.

REFERENCES

[1] J. Weiss, *Solar Energy Support in Germany: A Closer Look*, Jul. 2014. [Online]. Available: http://www.seia.org/sites/default/files/resources/1053germany-closer-look.pdf (visited on 04/16/2015).

[2] S. Sayeef, S. Heslop, D. Cornforth, T. Moore, S. Percy, J. K. Ward, A. Berry, and D. Rowe, "Solar intermittency: Australia's clean energy challenge," CSIRO, Tech. Rep., Jun. 2012, p. 198. [Online]. Available: https://publications.csiro.au/rpr/download?pid=csiro:EP121914&dsid=DS1 (visited on 04/18/2012).

[3] Ergon Energy and Energex, "Connection Standard: Small Scale Parallel Inverter Energy Systems up to 30 kVA," Tech. Rep. EX BMS4286 Ver 2, Jul. 2014, p. 32. [Online]. Available: https://www.ergon.com.au/__data/assets/pdf_file/0005/198698/STNW1170ver2-Connection-Standard-for-IES-up-to-30kVA.pdf (visited on 04/16/2015).

[4] Horizon Power, "Technical Requirements for Renewable Energy Systems Connected to the Low Voltage (LV) Network via Inverters," Tech. Rep. HPC-9FJ-12-0001-2012, Sep. 2014, p. 58. [Online]. Available: http://www.horizonpower.com.au/HPC_9FJ_12_0001_2012_Sta.pdf.

[5] Electric Power Research Institute (EPRI), "Common Functions for Smart Inverters, Version 3," EPRI, Palo Alto, CA, USA, Tech. Rep. 3002002233, 2013. [Online]. Available: http://www.epri.com/abstracts/Pages/ProductAbstract.aspx?ProductId=000000000001026809 (visited on 11/26/2012).

[6] Ausgrid, *Smart Grid, Smart City*, 2012. [Online]. Available: http://www.smartgridsmartcity.com.au/ (visited on 04/16/2015).

[7] S. Vorrath, *Solar milestone: 1,000,000 PV systems installed in Australia*, Apr. 2013. [Online]. Available: http://reneweconomy.com.au/2013/solar-milestone-1000000-pv-systems-installed-in-australia-44201 (visited on 04/16/2015).

[8] Bureau of Meteorology, *About One Minute Solar Data*, Jul. 2012. [Online]. Available: http://www.bom.gov.au/climate/data/oneminsolar/about-IDCJAC0022.shtml (visited on 04/16/2015).

[9] P. Jahangiri and D. Aliprantis, "Distributed volt/var control by pv inverters," *IEEE Transactions on Power Systems*, vol. 28, no. 3, pp. 3429–3439, 2013.

[10] F. Andrén, B. Bletterie, S. Kadam, P. Kotsampopoulos, and C. Bucher, "On the stability of local voltage control in distribution networks with a high penetration of inverter-based generation," *IEEE Transactions on Industrial Electronics*, vol. 62, no. 4, pp. 2519–2529, 2015. DOI: 10.1109/TIE.2014.2345347.

[11] M. E. Baran and F. F. Wu, "Optimal capacitor placement on radial distribution systems," *IEEE Transactions on Power Delivery*, vol. 4, no. 1, pp. 725–734, 1989.

[12] K. Turitsyn, P. Sulc, S. Backhaus, and M. Chertkov, "Distributed control of reactive power flow in a radial distribution circuit with high photovoltaic penetration," in *Proceedings of the IEEE PES General Meeting, PES 2010*, 2010.

[13] L. Collins and J. K. Ward, "Real and reactive power control of distributed pv inverters for overvoltage prevention and increased renewable generation hosting capacity," *Renewable Energy*, vol. 81, pp. 464–471, 2015.

[14] Y. Wang, P. Zhang, W. Li, W. Xiao, and A. Abdollahi, "Online overvoltage prevention control of photovoltaic generators in microgrids," *IEEE Transactions on Smart Grid*, vol. 3, no. 4, pp. 2071–2078, 2012.

[15] S. Alyami, Y. Wang, C. Wang, J. Zhao, and B. Zhao, "Adaptive real power capping method for fair overvoltage regulation of distribution networks with high penetration of pv systems," *IEEE Transactions on Smart Grid*, vol. 5, no. 6, pp. 2729–2738, 2014.

[16] K. Turitsyn, P. Sulc, S. Backhaus, and M. Chertkov, "Options for control of reactive power by distributed photovoltaic generators," *Proceedings of the IEEE*, vol. 99, no. 6, pp. 1063–1073, Jun. 2011, ISSN: 0018-9219. DOI: 10.1109/JPROC.2011.2116750.

[17] H. Khalil, *Nonlinear Systems*, 3rd. New Jersey: Prentice-Hall, 2002.

[18] R. Lincoln, *Pypower*, 2015. [Online]. Available: https://github.com/rwl/PYPOWER (visited on 04/10/2015).

[19] Olex, *Olex Overhead Design Manual*, 2012. [Online]. Available: %5Curl%7Bhttp://www.olex.com.au/Australasia/2012/OLC12641_AerialCat.pdf%7D.

[20] Clean Energy Council, *Grid-Connected Solar PV Systems - No Batttery Storage: Design Guidelines for Accredited Installers*, Jan. 2013. [Online]. Available: https://www.solaraccreditation.com.au/dam/solar-accred/installers/becoming-accredited/CEC-Accreditation-Design-Guidelines-Feb-2013.pdf (visited on 04/16/2015).